

Saturation modeling in a carbonate reservoir using capillary pressure based saturation height function: a case study of the SvK reservoir in the Y Field

P. Q. Lian · X. Q. Tan · C. Y. Ma ·
R. Q. Feng · H. M. Gao

Received: 24 May 2014 / Accepted: 2 February 2015 / Published online: 18 March 2015
© The Author(s) 2015. This article is published with open access at Springerlink.com

Abstract Because of the complex pore structure and the strong heterogeneity of the SvK carbonate reservoir in the Y Field, water saturation distribution and petrophysical properties, such as porosity, permeability and capillary pressure are difficult to be characterized. To solve this problem, a new method to interpret water saturation was presented. By this method, the relationships among porosity, permeability and different pore throat radii are fitted and a typical radius R30 (the pore aperture radius corresponding to 30 % of mercury saturation in a mercury penetration test) selected. By fitting the capillary pressure curves with Corey–Brooks function, the threshold pressure, the irreducible water saturation and the Corey exponent “*n*” of each capillary pressure curve can be determined, and the relationship between R30 and the threshold pressure, R30 and the irreducible water saturation, and R30 and the Corey exponent can all be fitted. If the R30 value is known, the threshold pressure, irreducible water saturation and Corey exponent can be calculated by the fitting equations; hence, the water saturation at a given height from FWL can be calculated by the Corey–Brooks function. The water saturation calculated by saturation height function is consistent with that of the well log interpretation and the error is less than by other methods. During the process of three-dimensional saturation modeling, an R30 criterion is presented to define rock types, six petrophysical rock types with different reservoir properties are distinguished and a link is set up between rock types and log responses by the KNN method. Logs are utilized to predict rock types of

non-cored wells according to this link, and a three-dimensional rock-type model is established by the Petrel software. R30 value of each grid can be calculated by R30 formula when three-dimensional porosity and permeability models are built with the restraint of rock-type model. Then, on the basis of the saturation height function, a three-dimensional water saturation model can be obtained.

Keywords Carbonate reservoir · Capillary pressure · Oil/water transition zone · Saturation height function

Introduction

Confirming the saturation distribution of a geologic model is a key step in the process of OOIP calculation of any integrated reservoir. The conventional and globally accepted method of saturation modeling is based on the capillary pressure curve data, which is obtained from the special core analysis (Jamiolahmady et al. 2007; Kumar et al. 2002; Zhao et al. 2008). The water saturation distribution above the FWL in an oil reservoir is controlled by the balance of capillary pressure and gravity forces, and when the capillary pressure is available, the water saturation at any given height will be known. Such relationship, known as the saturation height function, is used to estimate the saturation values away from the well locations and to calculate the hydrocarbons in place volumetrically (Buiting. 2007; Yan et al. 2008; Mohammad et al. 2012; Hu et al. 2012; Luo et al. 2013).

The saturation height functions can describe the drainage process during the hydrocarbon migration and are expressed as a relationship among the saturation, the height above the free water level and some model properties (commonly porosity and permeability). It can be used for the accurate

P. Q. Lian (✉) · X. Q. Tan · C. Y. Ma ·
R. Q. Feng · H. M. Gao
Sinopec Petroleum Exploration and Production Research
Institute, Beijing, China
e-mail: lianpq@163.com

modeling of water saturation, which has an effect on the geological reserve calculation, recoverable oil prediction and the future development planning. For a reservoir, the water saturation height functions are quite various. These variations are significant and difficult to estimate (Cuddy et al. 1993; Paul 2001; Kumar 2011; Seth et al. 2013). If the functions are not suitable for a reservoir, it will lead to inaccurate approximations during the process of the numerical simulation history matching for a field (Obinna et al. 2010; Joseph et al. 2012). Because of the wide range of lateral variations of the physical properties, carbonate reservoirs often have poor or no porosity/permeability correlation which will increase the complication in building capillary pressure models for non-cored wells (Buiting and Aramco 2011; Guo et al. 2007; Ibrahim 2009).

To interpret the water saturation more accurately, a new method has been presented to obtain a good match for complex carbonate reservoirs. In this method, typical radius R_{30} (the pore aperture radius corresponding to 30 % of mercury saturation in a mercury penetration test) is selected to describe the flow capacity of carbonates, and capillary pressure curves are used to establish the saturation height function by combining Corey–Brooks function and R_{30} . During the geological modeling process, the reservoir rock types are divided into six kinds, and each rock type has a different fluid distribution. After the permeability and porosity model were built, the three-dimensional water saturation model can be obtained on the basis of the saturation height function.

Field description

The Svk reservoir of Y Field is on the transition belt between the Zagros Fold Zone and the eastern margin of the Arab Platform. This field is an elongated anticline, which extends about 45 km in the north–south direction and about 15 km on the east–west direction. The mid-depth of the reservoir is 2,950 m, with the reservoir pressure of 4,800 psi. The storage space is dominated by the secondary porosity and the vugs, and there are few fractures in this reservoir. The average porosity is 12.04 %, and the average permeability is 5.87 mD.

Correlation of porosity, permeability and pore throat radii

Winland used the mercury injection–capillary pressure curves to develop an empirical relationship among the porosity, the permeability and the pore throat radius of the reservoir rock obtained from Spindle Field, Colorado. He tested 321 different water wet samples and correlated the relationship among the porosity, the air permeability and the pore throat radii corresponding to different mercury

saturations, and then found that the 35th percentile gave the best correlation. The 35th percentile equation to approximate pore throat sizes was used and published by Kolodzie (1980):

$$\log(R_{35}) = 0.732 + 0.588 \log(K_{\text{air}}) - 0.864 \log(\varphi), \quad (1)$$

where R_{35} is the pore aperture radius corresponding to the 35th percentile of mercury saturation in a mercury porosimetry test, K_{air} is uncorrected air permeability (mD) and φ is porosity (%).

After the Winland multiple regression analysis approach was published, this method was applied to many other areas. However, the best correlation of the porosity and the air permeability to pore throat radii does not always correspond to the mercury saturation of 35 %. Pittman (1992) developed a series of empirical equations to calculate the throat radii with the mercury saturations ranging from 10 to 75 % and found the best result at 25 %.

In the Y Field, a lot of capillary pressure experiments have been done. By applying Pittman's method on these data, we calculated the throat radii with the mercury saturations ranging from 10 to 85 % and found 30 % was the best percentile instead of 35 % (Table 1).

Saturation height function

Fitting for capillary pressure curves

At present, there are many methods to describe the relationship between the capillary pressure and the water saturation. Corey–Brooks function is an effective method for carbonate reservoirs. Corey–Brooks function was specially developed to describe capillary pressure curves. It represents both the long and the short transition zones well. Also, it fits most capillary curves well. Therefore, this method is the first choice.

The Corey–Brooks function is presented in the following form (Joseph et al. 2012):

$$S_w = S_{\text{wr}} + (1 - S_{\text{wr}}) \left(\frac{P_{\text{ce}}}{P_c} \right)^{\frac{1}{n}}, \quad (2)$$

where P_{ce} is the threshold pressure; P_c is the capillary pressure; S_{wr} is the irreducible water saturation; and n is the Corey exponent.

Before fitting the capillary curves by the Corey–Brooks function, the laboratory capillary pressure curves require the following corrections because of the following effects:

1. closure correction: because of rough surface of core sample, the voids created by surface irregularities will be filled with mercury before it truly enters the pore network, this effect can be identified by a steep change in slope at low saturations when the capillary pressure is plotted on a log-scale.

Table 1 Empirical equations of the Y Field

Mercury saturation (%)	Empirical equations	Correlation coefficient
10	$\log(R_{10}) = 0.678 + 0.509 \log(k) - 0.292 \log(\varphi)$	0.807
15	$\log(R_{15}) = 0.668 + 0.520 \log(k) - 0.449 \log(\varphi)$	0.850
20	$\log(R_{20}) = 0.647 + 0.517 \log(k) - 0.550 \log(\varphi)$	0.874
25	$\log(R_{25}) = 0.631 + 0.513 \log(k) - 0.626 \log(\varphi)$	0.886
30	$\log(R_{30}) = 0.611 + 0.509 \log(k) - 0.694 \log(\varphi)$	0.895
35	$\log(R_{35}) = 0.590 + 0.502 \log(k) - 0.751 \log(\varphi)$	0.887
40	$\log(R_{40}) = 0.571 + 0.495 \log(k) - 0.803 \log(\varphi)$	0.867
45	$\log(R_{45}) = 0.556 + 0.487 \log(k) - 0.851 \log(\varphi)$	0.838
50	$\log(R_{50}) = 0.537 + 0.477 \log(k) - 0.894 \log(\varphi)$	0.812
55	$\log(R_{55}) = 0.519 + 0.466 \log(k) - 0.934 \log(\varphi)$	0.790
60	$\log(R_{60}) = 0.499 + 0.454 \log(k) - 0.971 \log(\varphi)$	0.771
65	$\log(R_{65}) = 0.479 + 0.442 \log(k) - 1.006 \log(\varphi)$	0.756
70	$\log(R_{70}) = 0.461 + 0.427 \log(k) - 1.040 \log(\varphi)$	0.743
75	$\log(R_{75}) = 0.444 + 0.412 \log(k) - 1.071 \log(\varphi)$	0.734
80	$\log(R_{80}) = 0.426 + 0.396 \log(k) - 1.101 \log(\varphi)$	0.728
85	$\log(R_{85}) = 0.407 + 0.378 \log(k) - 1.131 \log(\varphi)$	0.727

2. confining stress correction: under reservoir conditions the rock suffers a different stress regime than during laboratory capillary curve measurements, the latter usually being made under atmospheric conditions. Such stress relief increases both porosity and permeability, and affects capillary curve-derived saturations.

3. clay correction: the existence of clays can alter the effective water saturation, therefore, the laboratory capillary pressure curves should be corrected based on experimental data.

4. wettability and interfacial tension correction: since the laboratory fluid system does not have the same wettability and surface tension as the reservoir system, it becomes necessary to convert laboratory capillary pressure to reservoir capillary pressure (Fig. 1).

Using the Corey–Brooks function to fit the capillary pressure curves and the threshold pressure, irreducible water saturation and Corey exponent n can be obtained, as shown in Fig. 2.

After all capillary curves from core samples have been smoothed and fitted by the Corey–Brooks function, a set of Corey parameters, i.e., the threshold pressure, the irreducible water saturation and the Corey exponent, can be derived. Then, the relationship to estimate Corey parameters from some rock properties of reservoir can be obtained.

Saturation height function model

Figure 3 shows the relationship among R_{30} , the threshold pressure, the irreducible water saturation and the Corey exponent n in semi-log plots. It can be found that with the increase of the critical radius R_{30} , the threshold pressure

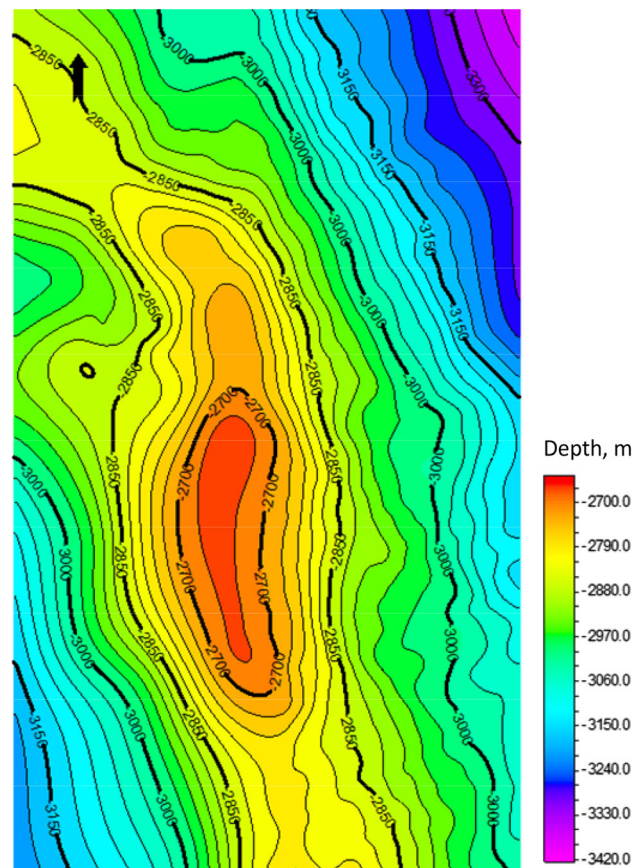


Fig. 1 Structural model of the SvK reservoir

and the irreducible water saturation decrease and the Corey exponent n increases. The formulas between R_{30} and the other parameters are presented by fitting the test data with the exponential function:

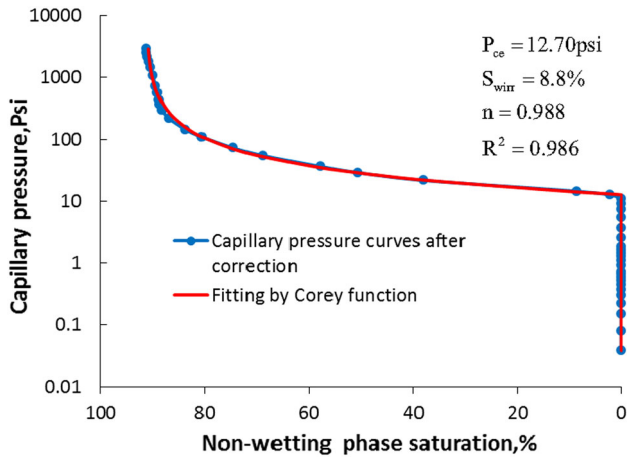


Fig. 2 Capillary pressure curve fitting by Corey–Brooks function

$$P_{ce} = 6.0616R_{30}^{-0.797}, \tag{3}$$

$$S_{wi} = 14.397R_{30}^{-0.1105}, \tag{4}$$

$$n = 1.0529R_{30}^{0.2342}. \tag{5}$$

On the basis of those formulas, the initial water saturation can be calculated by selecting a favorable R30.

Before the development of reservoirs, the fluid is quiescent and the water saturation distribution above the FWL in this oil reservoir is controlled by the balance of the capillary pressure and the gravity force. The value of the capillary pressure depends on the pore throat radius, and the gravity force depends on the density difference between water and oil. According to Corey–Brooks function, the saturation height function can be obtained by combining the height above the free water level, the reservoir depth and the pore throat size. The equation can be expressed in the following form:

$$S_w = S_{wr}(R_{30}) + (1 - S_{wr}(R_{30})) \left(\frac{P_{ce}(R_{30})}{\Delta\rho g \cdot \text{HAFWL}} \right)^{\frac{1}{n(R_{30})}}, \tag{6}$$

where $\Delta\rho$ is the density difference between water and oil, g/cm^3 ; g is acceleration of gravity, m/s^2 ; and HAFWL is height above free water level, m .

Comparison between water saturation obtained from logging and saturation height function

Fitting for saturation from logs

For the wells, the water saturation can be obtained by interpreting the wireline logging. One purpose of this research is to build up the water saturation profile that matches the interpreted electrical log saturation profiles.

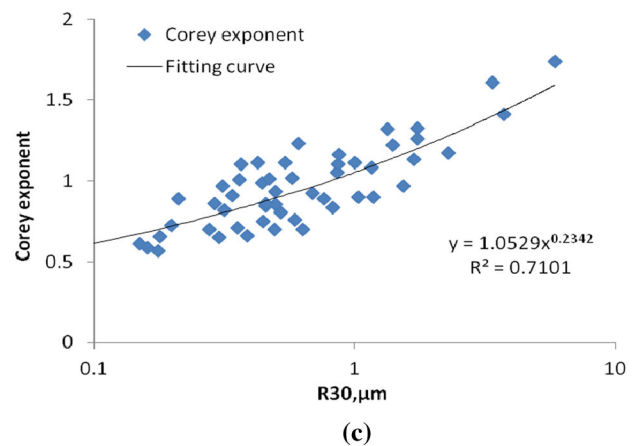
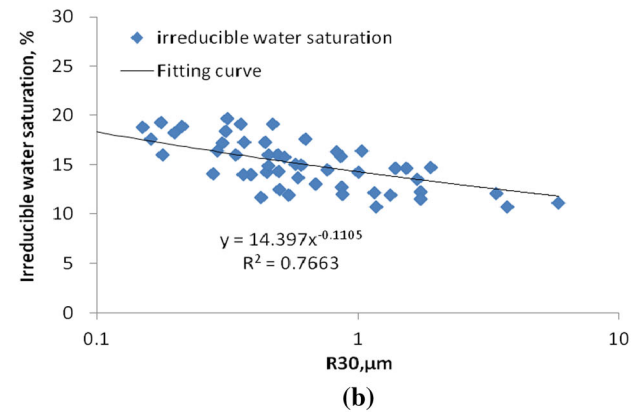
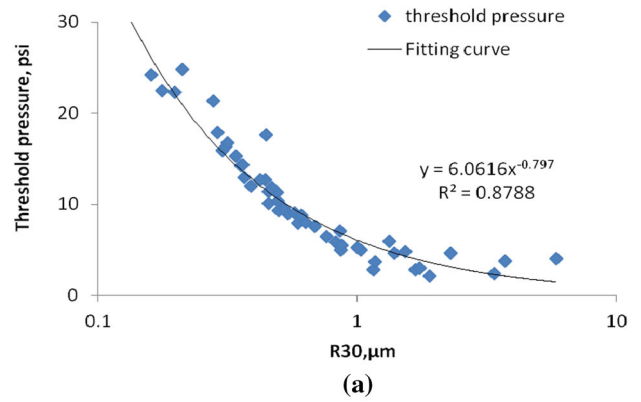


Fig. 3 Relationship among R30 and threshold pressure, irreducible water saturation and Corey exponent. **a** Relationship between R30 and threshold pressure, **b** relationship between R30 and irreducible water saturation and **c** relationship between R30 and Corey exponent

The above method is used to determine the saturation profile of A1 and A2 wells in the SvK reservoir. The results match the saturation profiles interpreted from the electrical logs very well as shown in Fig. 4.

Figure 5 is the cross plot of the water saturation interpreted by logging and the one calculated by the saturation height function of the A1 well. It indicates that these two

Fig. 4 Comparison between water saturation interpreted by logging and calculated by saturation height function. **a** A1, **b** A2

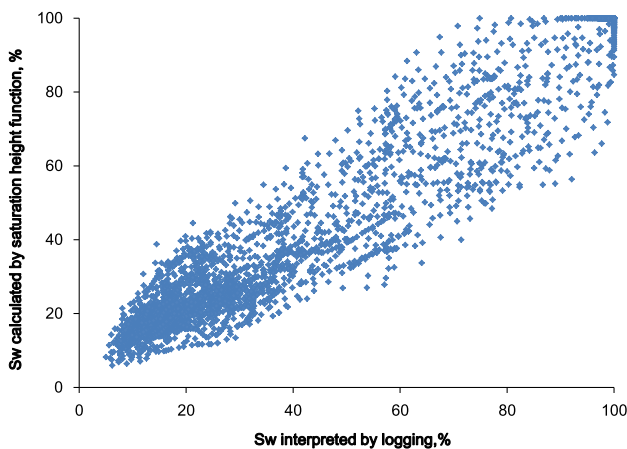
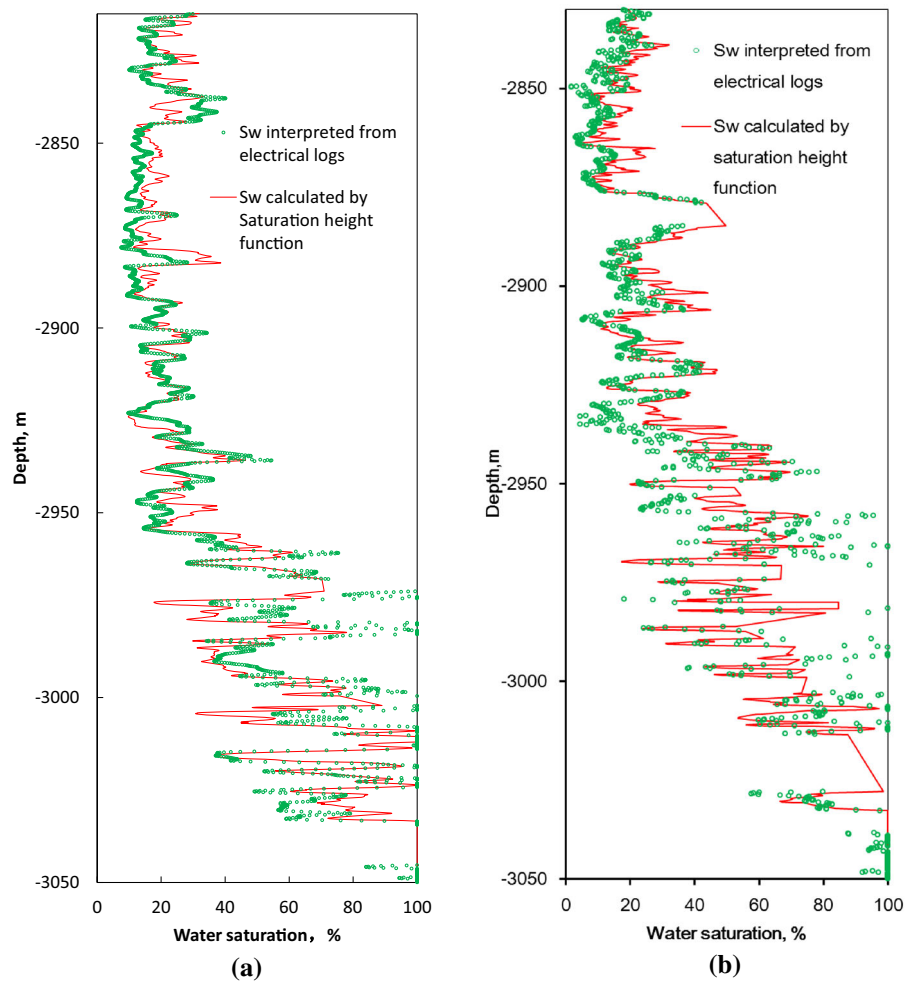


Fig. 5 Cross plot between logging water saturation and calculated saturation by saturation height function

kinds of water saturation coincide with each other very well as the points distribute along the diagonal line of the plot.

Fitting for saturation from logs

To elaborate on the accuracy of different saturation height functions, two criteria have been made to quantify the accuracy of each method:

1. Average absolute percentage deviation, AAD %, which is calculated by using the following equation (Mohammad et al. 2012):

$$AAD\% = \frac{\sum_{j=1}^n \frac{|(S_w)_{core} - (S_w)_{log}|}{(S_w)_{log}}}{n} \times 100. \tag{7}$$

2. The standard error of estimate (Mohammad et al. 2012)

$$SEE = \sqrt{\frac{\sum_{j=1}^n [(S_w)_{core} - (S_w)_{log}]^2}{n - 1}}, \tag{8}$$

where subscripts (log) and (core) denote the values obtained from log and core analyses, respectively.

Table 2 shows the accuracy of the saturation height function in this paper and two other methods which can be

Table 2 Comparison between the method in this paper and other methods

Methods	AAD (%)	SEE
Leverett J function	47.3	0.236
Cuddy method	37.1	0.197
Saturation height function	26.4	0.115

found in some literature. It is found that the saturation height function method produces fewer errors than the other methods; thus, it is the best among these three.

Three-dimensional saturation model

The saturation height function presented above can be used to establish the water saturation model between wells. Firstly, the R30 method can be used to identify the rock types of carbonate reservoirs. Secondly, a link is set up between rock types and log responses, and then the logs are utilized to predict rock types of non-cored wells according to this link. With the rock types of each well known, a 3D rock-type model will be established through sequential indicator simulation. The R30 value of each grid can be calculated by the R30 formula when a three-dimensional porosity and permeability model is built up with the restraint of the rock-type model. Then the threshold pressure, irreducible water saturation and Corey exponent can be obtained from Eqs. (3)–(5). The water saturation of each grid can be obtained from Eq. (6).

Classification of rock types

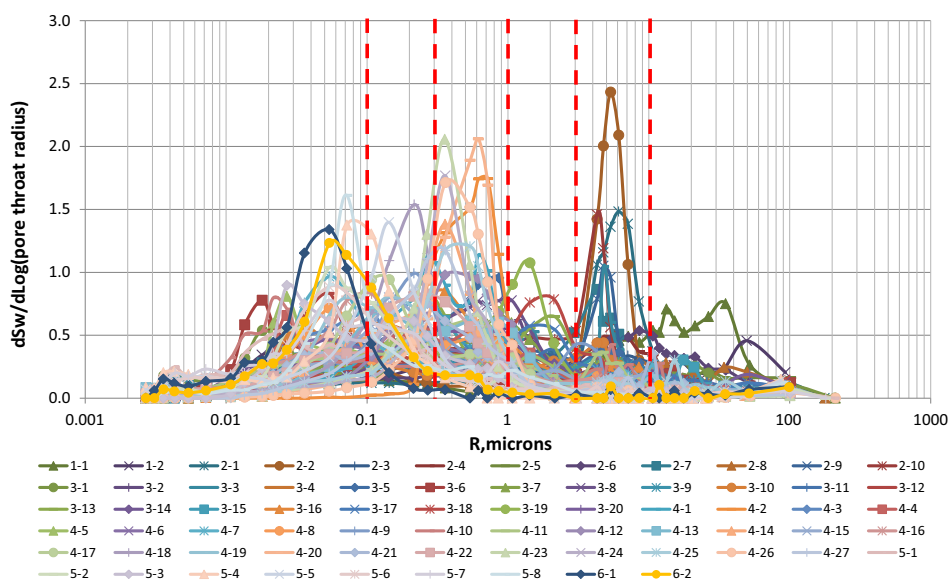
As shown in Fig. 6, because of the strong heterogeneity in the Svk carbonate reservoir, the peak of the pore throat

derived from the MICP test shows quite various distributions. Based on the pore throat distribution of plugs, five pore throat radii are used to define rock types, and the typical radii are $r = 0.1 \mu\text{m}$, $r = 0.3 \mu\text{m}$, $r = 1.0 \mu\text{m}$, $r = 3.0 \mu\text{m}$ and $r = 10.0 \mu\text{m}$. Six petrophysical flow units with different reservoir performances can be distinguished and clearly defined as: (1) rock type 1: $r \geq 10.0 \mu\text{m}$; (2) rock type 2: $3.0 \leq r < 10.0 \mu\text{m}$; (3) rock type 3: $1.0 \leq r < 3.0 \mu\text{m}$; (4) rock type 4: $0.3 \leq r < 1.0 \mu\text{m}$; (5) rock type 4: $0.1 \leq r < 0.3 \mu\text{m}$; (6) rock type 5: $r < 0.1 \mu\text{m}$.

Capillary pressure data are useful in characterizing rock types because it is an indication of pore throat size distribution within one rock type. Figure 7 shows different capillary pressure curves of each rock type in the Svk reservoir. We could find that there were some clear banding based on the R30 method. When the mercury saturation is 30 %, there is one turning point on the capillary pressure curve and the “width” of the capillary pressure curve set becomes narrow. At the mercury saturation of 30 %, the pore spaces dominate the flow behavior, while the rest of the pore spaces only contribute to storage and not to the flow; this further verifies the reliability of the R30 method. As the rock number becomes larger, the flattened segment of the capillary pressure curve becomes higher.

Figure 8 is the thin-section photos of each rock type, and their main textures are different for the six major rock types. From group (a) to group (f), the rock quality becomes worse. Rock type 1 develops fractures that lead to high flow conductivity and high permeability. Rock type 2 develops lots of vugs, which connect with each other and form flow network. Rock type 6 is very tight with low porosity so that the fluid cannot move in this rock type. Therefore, it could act as a barrier. The textures of rock

Fig. 6 Pore throat distribution of plugs



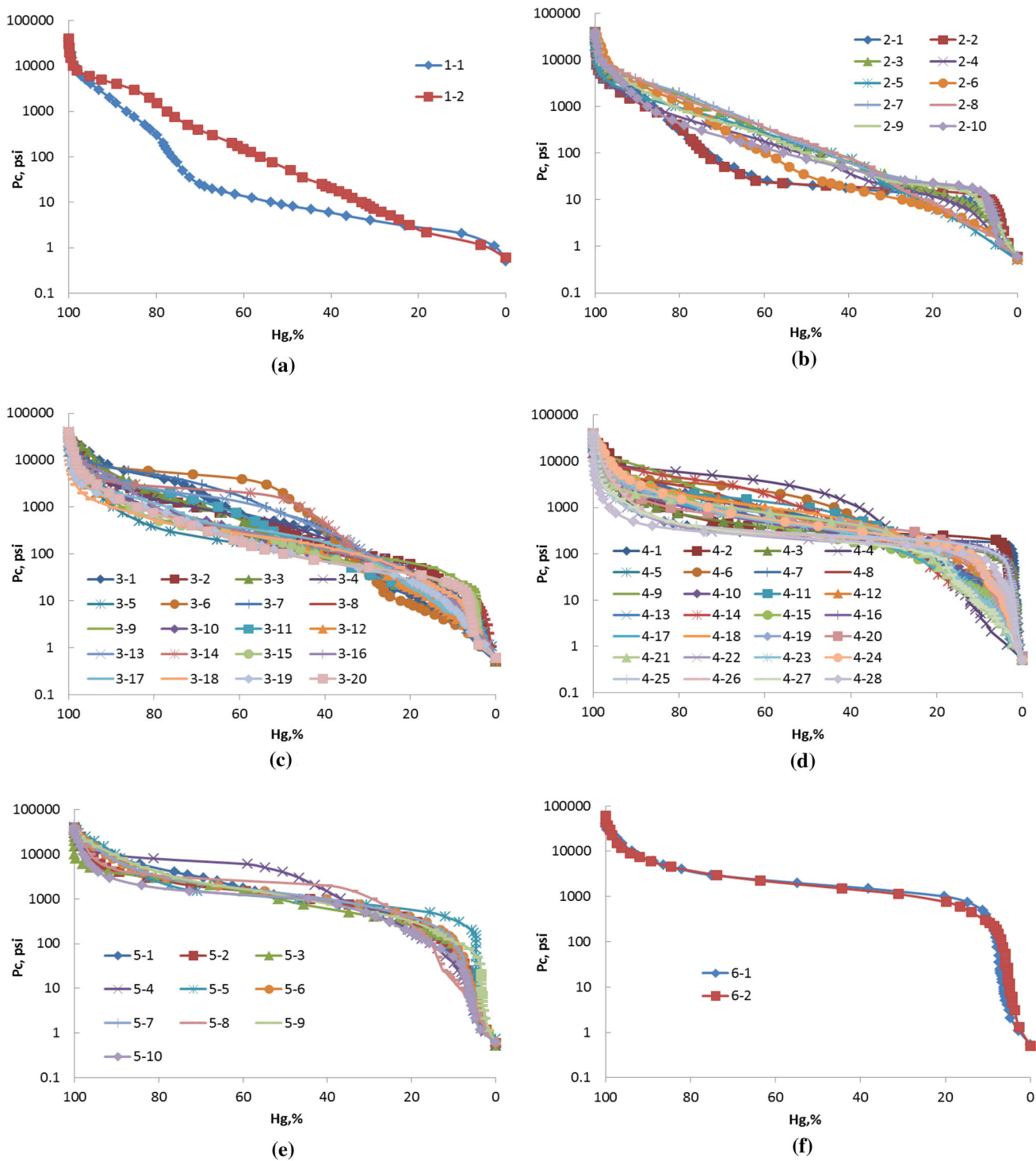


Fig. 7 Capillary pressure curves of each rock type. **a** Rock type 1, **b** rock type 2, **c** rock type 3, **d** rock type 4, **e** rock type 5 and **f** rock type 6

type 2 to rock type 5 are between those of rock type 2 and rock type 6.

There are 1,640 samples from nine cored wells, of which the porosities and permeabilities were tested in the laboratory. The samples are divided into six petrophysical facies as shown in Fig. 9 by five typical lines. The porosity

and permeability relationship can be obtained by using data of each rock type. Table 3 shows the average porosity, the permeability and the relationships between porosity and permeability of each rock type in the Svk reservoir. We can see that the average permeability and porosity become larger as the rock properties become better, and each rock

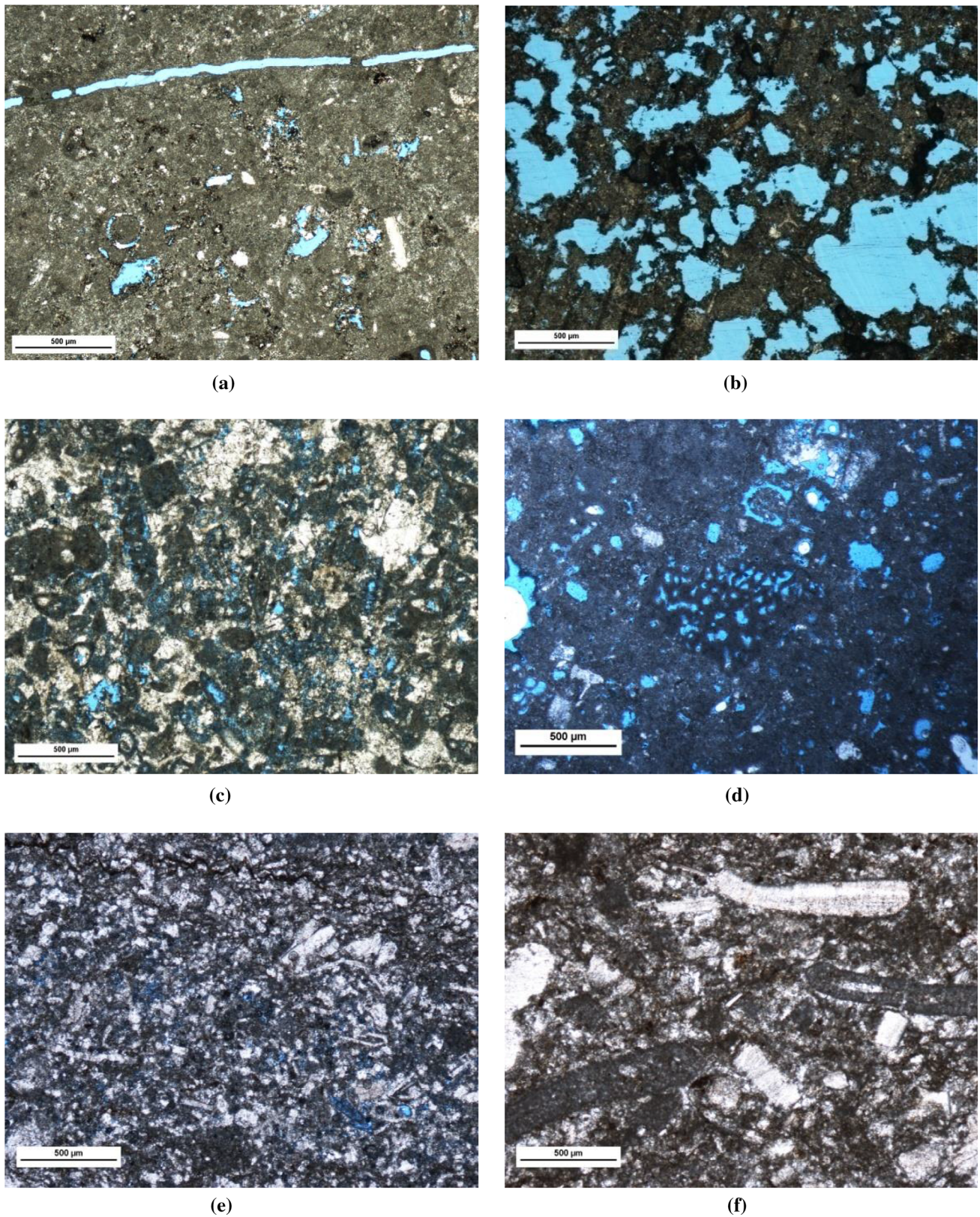


Fig. 8 Thin section photos of each rock type. **a** Plug 1–1, 4,282.69 m, PPL, rock type 1, **b** plug 2–6, 4,261.55 m, PPL, rock type 2, **c** plug 3–12, 4,135.74 m, PPL, rock type 3, **d** plug 4–7,

4,150.91 m, PPL, rock type 4, **e** plug 5–9, 4,127.27 m, PPL, rock type 5, **f** plug 6–1, 4,122.67 m, PPL, rock type 6

Fig. 9 Rock type classification

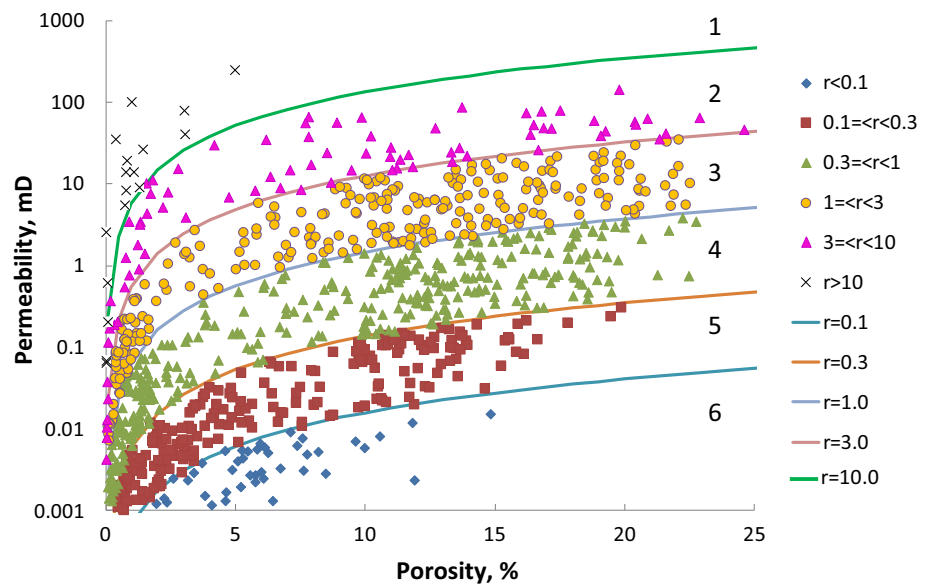


Table 3 Parameters of each rock type

Rock type	R30 (μm)	Average porosity (%)	Average permeability (mD)	<i>K</i> & Φ	<i>R</i> ²
1	$r \geq 10.0$	1.21	124.35	$K = 19.076\Phi^{1.0431}$	0.7341
2	$3.0 \leq r < 10.0$	11.87	26.71	$K = 1.4015\Phi^{1.2853}$	0.9334
3	$1.0 \leq r < 3.0$	10.05	5.58	$K = 0.1749\Phi^{1.3659}$	0.9021
4	$0.3 \leq r < 1.0$	8.64	0.586	$K = 0.0176\Phi^{1.4183}$	0.9011
5	$0.1 \leq r < 0.3$	6.12	0.041	$K = 0.0022\Phi^{1.3722}$	0.8569
6	$r < 0.1$	4.51	0.003	$K = 0.0004\Phi^{1.1005}$	0.6858

type has different fitting equations with reasonably high correlation coefficient.

Three-dimensional geological model

To predict the rock types of uncored intervals or uncored wells, the KNN algorithm is used to establish a link between the rock types and the logging parameters (Francesconi et al. 2009; Michel et al. 2009).

There are many parameters on the log curves, such as the shale content (Vsh), resistivity (RT, RS), compensated neutron logging (CNL), density (DEN), sonic transit time (DT), porosity (POR) and water saturation (*S_w*). All the interpreted logs are normalized by using the following equation:

$$\bar{\delta} = \frac{\delta - \delta_{\min}}{\delta_{\max} - \delta_{\min}}, \tag{9}$$

where $\bar{\delta}$ is the normalized log value, and δ_{\min} and δ_{\max} are the minimum and maximum values of the δ log data, respectively. The values of the normalized logs are extracted at the same depth as the core plugs, and the normalized log value and petrophysical facies number of plug are regarded

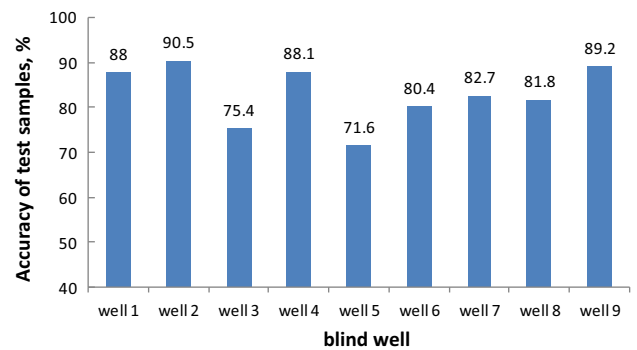


Fig. 10 The predicted accuracy when well *i* is taken as blind well

as one sample. The log value is a known parameter for all wells and the petrophysical facies number can be trained by the known samples.

We use an arbitrary well in the nine cored ones as the blind well and the samples from the other eight wells as the training samples. After comparing the predicted results and the measured ones in the laboratory, the accuracy of the KNN algorithm can be confirmed. As shown in Fig. 10, the predicted accuracy is greater than 70 %, ranging from 71.6

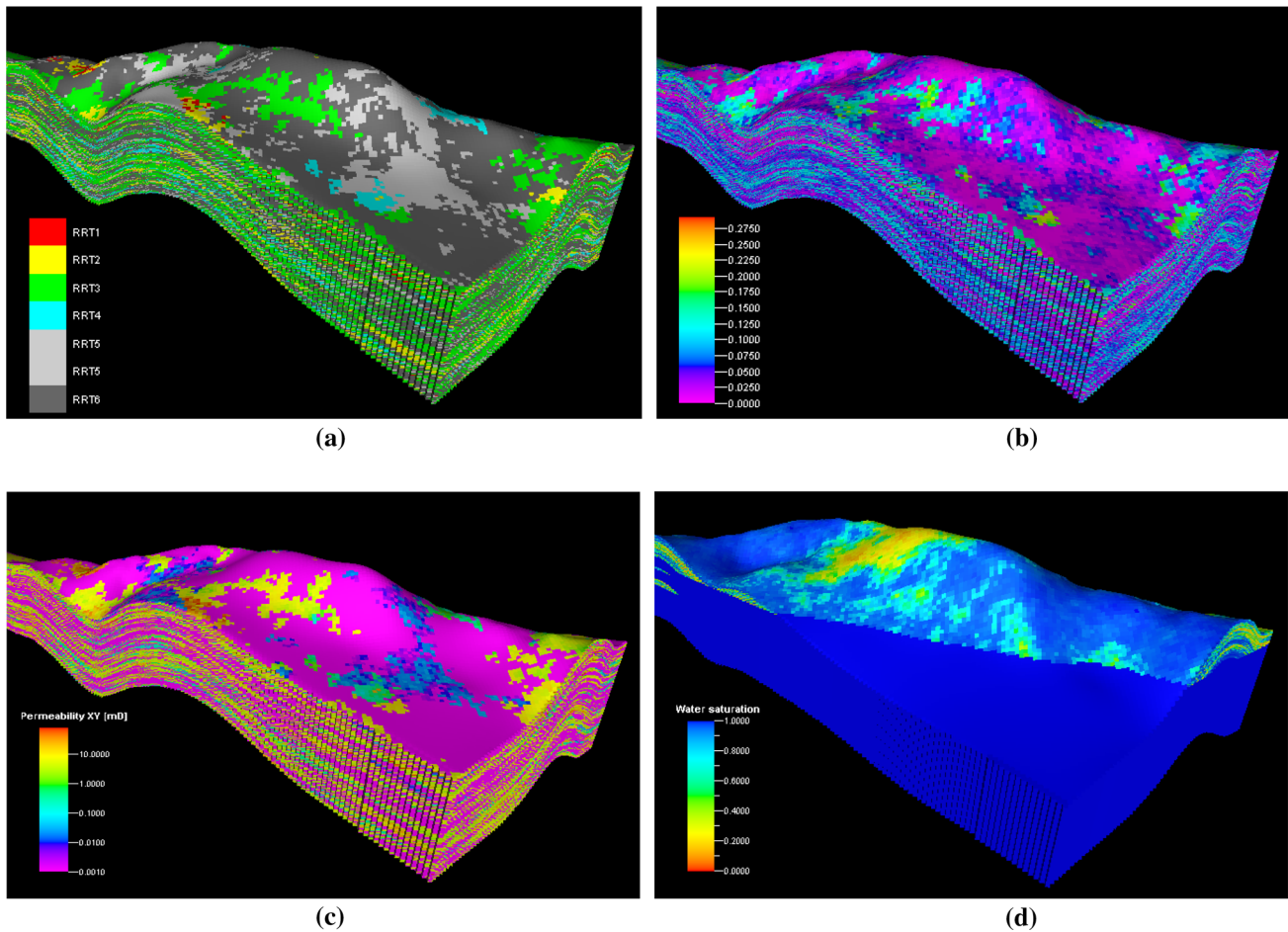


Fig. 11 Three-dimensional rock-type model. **a** Rock-type model, **b** permeability model, **c** porosity model and **d** water saturation model

to 90.5 %, and the average predicted accuracy is 83.1 %. The predicted results can be used to judge the rock type of the reservoir.

Based on the above study on the RRT scheme, Well-derived RRT curves for current wells are used to create the 3D model by the Petrel software. After the rock types of all wells are predicted, a 3D rock-type model is established by the sequential indicator simulation as shown in Fig. 11a. Six RRTs for the SvK reservoir are defined, respectively, and from RRT1 to RRT6 the reservoir properties become worse gradually.

Once the reservoir rock type has been chosen and distributed in the 3D volume, the next task is to generate properties such as porosity and permeability. These properties are originally derived from the rock types and the well logs (Gomes et al. 2008; Salman and Bellah 2009; Tan et al. 2013). By integrating the rock type and the well log data, a 3D porosity model will be built (Fig. 11b). The final permeability model was obtained on the basis of the permeability–porosity relationships (shown in Table 3) for each rock type as shown in Fig. 11c. After the three-dimensional porosity and permeability model was built, the

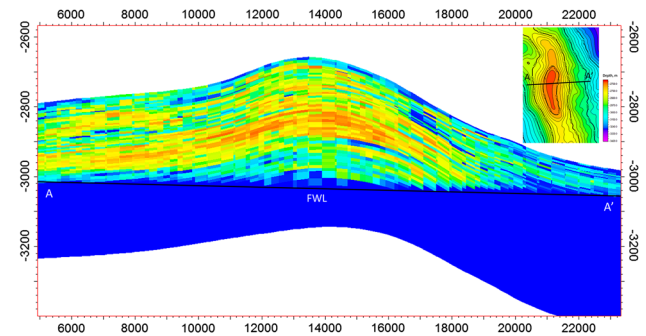


Fig. 12 Initial water saturation distribution of the SvK reservoir

R30 formula was used to calculate the R30 value of each grid. Then the threshold pressure, irreducible water saturation and the Corey exponent can be obtained from Eqs. (3)–(5). Water saturation of each grid can be obtained from Eq. (6), and Fig. 11d shows the three water saturation models.

Figure 12 shows the profile of water saturation distribution which is derived from the saturation height function. The oil/water transition zone is apparently displayed in the

model. As the distance gets farther from the free water level, water saturation becomes lower. Additionally, rock quality also has an effect on water saturation. With the increase of the rock-type number, the rock quality becomes better and the water saturation becomes higher. The saturation height function can be used in the numerical simulation model directly. Therefore, the reserve of the geological model and the numerical model is unity and the calculating accuracy of the fluid model is improved.

Conclusions

Saturation distribution of a geologic model is very important for OOIP calculation of reservoirs. A precise prediction of the saturation model could give us a better understanding of the underground reservoir fluid flow and also improve oil recovery. In this study, we provide an improved new method to calculate saturation distribution according to pore throat distribution and draw the following conclusions:

1. The relationships among porosity, permeability and different pore throat radii were fitted and the typical pore throat radius R30 was selected. The relationship among R30-threshold pressure P_{ce} , the irreducible water saturation and the Corey exponent was obtained. Then, single well initial water saturation was calculated by selecting the relevant parameters according to the pore throat radius, and the result was consistent with the well log interpretation result.

2. The R30 method is presented to define rock types. Six petrophysical flow units with different reservoir properties can be distinguished and each rock type has similar capillary pressure curves. When the mercury saturation is equal to 30 %, the capillary pressure curves have a turning point and the “width” of a set of capillary pressure curves becomes narrow.

3. A link was set up between rock types and the log responses. Logs were utilized to predict rock types in non-cored wells according to this link, and a three-dimensional rock-type model was established. With the restraint of the rock-type model, a three-dimensional porosity and permeability model can be built. The R30 value of each grid can be calculated by the R30 formula.

4. By using the saturation height function, a three-dimensional water saturation model can be obtained. The model has an obvious oil–water transition zone, and the water saturation decreases with the increase of the height from the free water level. Besides, with the change of the model internal physical properties of rock, the water saturation also shows different characteristics.

Open Access This article is distributed under the terms of the Creative Commons Attribution License which permits any use,

distribution, and reproduction in any medium, provided the original author(s) and the source are credited.

References

- Buiting J (2007) Fully upscaled saturation-height functions for reservoir modeling based on Thomeer’s method for analyzing capillary pressure measurements. In: Paper SPE 105139 presented at the 15th SPE Middle East oil & gas show and conference held in Bahrain International Exhibition Centre, Kingdom of Bahrain
- Buiting J, Aramco S (2011) Upscaling saturation-height technology for Arab carbonates for improved transition-zone characterization. *SPE Reserv Eval Eng* 14(1):11–24
- Cuddy S, Steele R, Allinson G (1993) A simple, convincing model for calculating water saturations in southern North Sea gas fields. In: PWLA 34th annual logging symposium
- Francesconi A, Bigoni F, Balossino P et al (2009) Reservoir rock types application—Kashagan. In: Paper 125342 presented at SPE SPE/EAGE reservoir characterization and simulation conference, 19–21 October 2009, Abu Dhabi
- Gomes JS, Ribeiro MT, Christian J (2008) Carbonate reservoir rock typing—the link between geology and SCAL. In: Paper SPE 118284 presented at Abu Dhabi international petroleum exhibition and conference
- Guo G, Diaz MA, Paz F (2007) Rock typing as an effective tool for permeability and water-saturation modeling: a case study in a clastic reservoir in the oriente basin. *SPE Reserv Eval Eng* 10(6):730–739
- Hu Y, Yu X, Chen G (2012) Classification of the average capillary pressure function and its application in calculating fluid saturation. *Pet Explor Dev* 39(6):733–738 (in Chinese)
- Ibrahim HW (2009) Developing generalized capillary pressure curves and saturation height function for Shuaiba carbonate reservoir in field A. In: Paper SPE 136191 presented at the SPE annual technical conference and exhibition held in New Orleans, 4–9 October 2009
- Jamiolahmady M, Sohrabi M, Tafat M (2007) Estimation of saturation height function using capillary pressure by different approaches. In: Paper SPE 107142 presented at EUROPEC/EAGE conference and exhibition, London
- Joseph J, Elizabeth A, Daniel A (2012) A saturation height function model derived from capillary pressure, Lower Etchegoin/Williamson Reservoir, Lost Hills Field. In: Paper SPE 153594 presented at SPE western regional meeting, Bakersfield
- Kolodzie SJ (1980) Analysis of pore throat size and use of the Waxman–Smits equation to determine OOIP in spindle field. In: Colorado, paper SPE 9382 presented at SPE annual technical conference and exhibition, 21–24 September 1980, Dallas
- Kumar R (2011) Development of saturation height functions for a multilayered carbonate reservoir of an Indian Offshore Field. In: The 9th Biennial international conference and exposition on petroleum geophysics, held at Hyderabad
- Kumar R, Cherukupalli PK, Lohar BL (2002) Saturation modeling in a multilayered carbonate reservoir using log-derived saturation-height function. In: Paper SPE 75213 presented at SPE/DOE improved oil recovery symposium, Tulsa
- Luo H, Tang D, Tang Y (2013) Study on prediction of oil water contact in carbonate reservoir with capillary pressure data. *Pet Geol Recov Effic* 20(2):71–73 (in Chinese)
- Michel R, Francois U, Emmanuelle P et al (2009) Pore to grid carbonate rock-typing. In: Paper IPTC 13120 presented at the international petroleum technology conference held in Doha, 7–9 December 2009

- Mohammad H, Rafael K, Nasser A (2012) Water saturation modeling in Khafji carbonate reservoir. In: Paper SPE 161427 presented at the 20th international offshore and polar engineering conference, 20–25 June 2012, Beijing
- Obinna C, Roya S, Osemoahu AO (2010) Saturation modeling in a geological complex clastic reservoir using log derived saturation height function: a case study of the E2 reservoir, Era Eko field in the Niger Delta. In: Paper SPE 140635 presented at the 34th annual SPE international conference and exhibition held in Tinapa-Calabar, 31 July–7 August 2010
- Paul FW (2001) Scale effects on the application of saturation-height functions to reservoir petrofacies units. *SPE Reserv Eval Eng* 4(5):430–436
- Pittman ED (1992) Relationship of porosity and permeability to various parameters derived from mercury injection-capillary pressure curves for sandstone. *AAPG Bull* 76:191–198
- Salman SM, Bellah S (2009) Rock typing: an integrated reservoir characterization tool to construct a robust geological model in Abu Dhabi carbonate oil field. In: Paper SPE 125498 presented at SPE/EAGE reservoir characterization and simulation conference
- Seth K, Beales V, Kawasaki A (2013) Saturation height function in a field under imbibition: a case study. In: Paper SPE 165880 presented at the SPE Asia Pacific oil & gas conference and exhibition held in Jakarta
- Tan X, Lian P, Qiu M, Li Y, Dong G (2013) Rock type-constrained geological modeling of carbonate reservoirs: a case study of carbonate reservoir A in the Zagros Basin. *Oil Gas Geol* 34(4):558–563 (in Chinese)
- Yan W, Tian Z, Ma L (2008) Evaluation on oil saturation of carbonate reservoir in H oilfield using capillary pressure and logging data. *Petrol Geol Oilfield Dev Daqing* 27(3):121–123 (in Chinese)
- Zhao G, Zhu J, Guan L (2008) Method of applying capillary pressure data to calculate initial oil saturation. *J China Univ Pet* 22(4):38–41 (in Chinese)